ELSEVIER

Physica D 90 (1996) 293–305

PHYSICA D

# Concentric decomposition during rapid compact growth

Menahem Zukerman, Raz Kupferman, Ofer Shochet, Eshel Ben-Jacob

*School of Physics and Astronomy, Raymond and Beverly Sackler Faculty of Exact Sciences, Tel Aviv University, Tel Aviv 69978, Israel*

Received 4 April 1995; revised 22 June 1995; accepted 26 July 1995
Communicated by L. Kramer

**Abstract**

We study the propagation of compact superheated solid in the large undercooling limit using the phase-field model. Below a critical undercooling, the superheated solid decomposes into solid and liquid domains, either in the form of liquid droplets or in periodic structures of concentric rings. For the latter, a one-dimensional analysis provides an excellent estimate for the propagation velocity and for the wavelength. Both numerical and approximate analytical expressions are obtained.

*PACS:* 61.50.Cj 64.60.-i 64.70.Dv 81.10.Fq 81.30.Fb

## 1. Introduction

During the past decade a considerable progress has been achieved in the understanding of interfacial patterning [1–4]. Initially, the focus was on the formation of isolated growth elements (e.g., dendrites, fingers and bubbles). This approach was motivated by the need to explain the existing experiments on steady-state dendritic and fingering growth. Solidification experiments, for example, were mainly performed in the limit of low undercooling [5]. Under such conditions, neighboring branches are almost non-interacting as the average solid–liquid fraction is equal to the dimensionless undercooling [6,7]. Technically, the investigation of steady-state growth of isolated patterns provides an enormous simplification compared to the consideration of the full time-dependent behavior of global morphologies. In particular, this approach led to the discovery of the singular nature of the microscopic interfacial dynamics, and to the formulation of solvability criterions for the existence of different types of isolated growth elements [8–10].

Another case which has received much attention is the opposite limit of very large undercooling. For $\Delta > 1$, all the latent heat is absorbed by the solidification front, hence, the interface can remain stable and form a compact structure. In this regime the problem can easily be solved as the solution is a quasi-one-dimensional steady-state.

Clearly, the most interesting and challenging regime is the intermediate case of finite (but not too large) undercooling. When the interactions between branches become dominant, a subtle self-organization mechanism leads to the formation of a regular well-defined envelope on the global scale, even when the growth is very noisy and irregular on the scale of the individual branches [6]. This envelope remains shape preserving and propagates at constant velocity. Moreover, the geometrical characterization of the envelope seems to be correlated with the internal branching structure. Specifically, the envelope was found to be convex for tip-splitting growth, while concave for dendritic


*SSDI* 0167-2789(95)00240-5

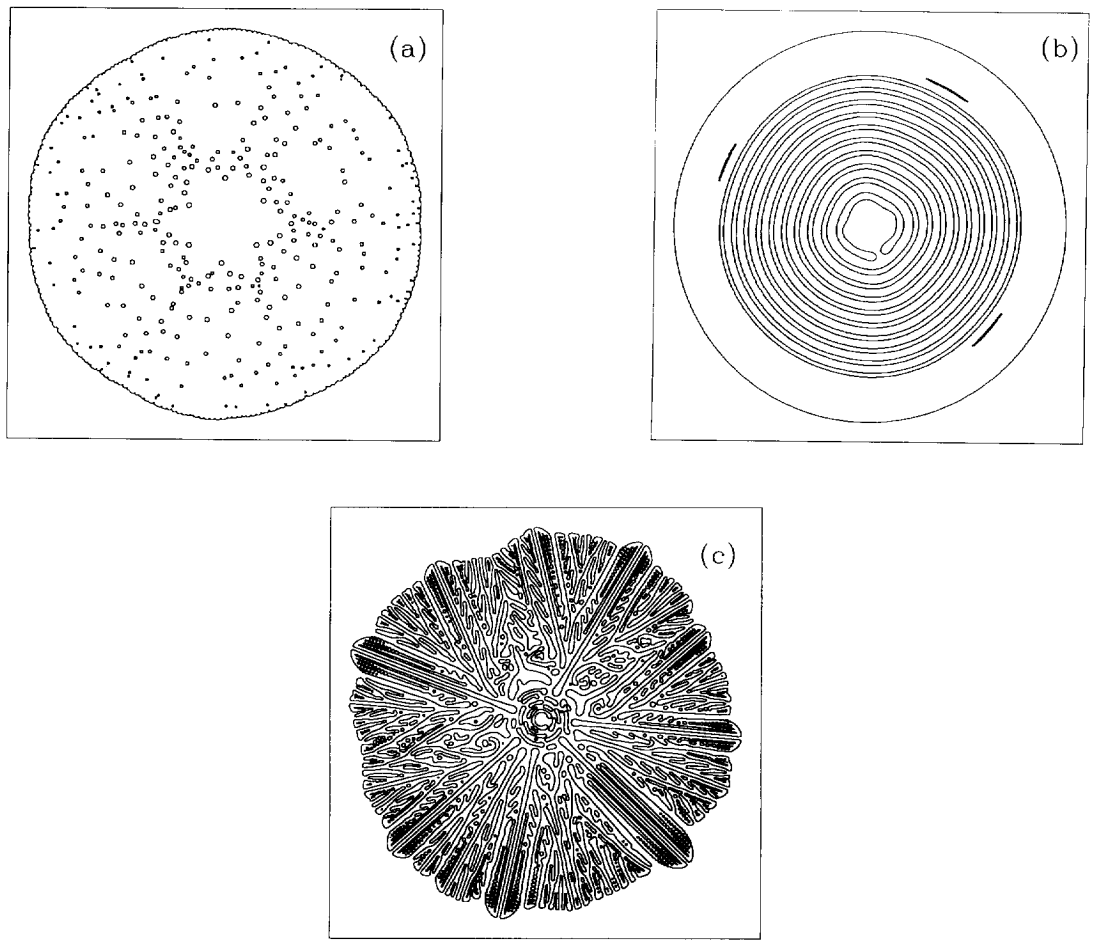


Fig. 1. Numerical simulations of the two-dimensional phase-field model. The lines represent $\phi = 0.5$ contour lines. (a) Array of droplets behind a compact solid front obtained for $\epsilon = 0.2$, $\lambda = 10$ and $\Delta = 0.9$. (b) A typical example of concentric rings structure for $\epsilon = 0.35$, $\lambda = 10$ and $\Delta = 0.65$. The rings start with the nucleation of droplets which then propagate to fill the entire circumference. (c) Tip splitting growth obtained for $\epsilon = 0.35$, $\lambda = 10$ and $\Delta = 0.55$.

growth [6]. In order to investigate this growth regime, it is necessary to resolve the time-dependent behavior of the fully-developed structure. In the absence of appropriate analytical tools, such treatment has been restricted so far mainly to the framework of algorithmic computational models, and recently, it has also been possible to achieve large-scale numerical simulations of deterministic growth models [11–15].

In Ref. [15], numerical simulations of the phase-field model were performed in the large undercooling limit. In particular, a new pattern was found to emerge for levels of undercooling close to one. For values of $\Delta$ down to 0.85, the solidification front remains compact. Energetical considerations imply that compact growth below unit undercooling gives rise to a superheated solid. Such state turns out to be unstable with respect to propagating wave-fronts of solid–liquid decomposition. In the simulations of Ref. [15], it yielded arrays of liquid droplets forming behind the solidification front (Fig. 1a). Solid–liquid decomposition can also appear in the form of a periodic structure of concentric rings (Fig. 1b). Below a critical value of undercooling, the concentric pattern breaks down, and a transition to radial branching occurs (Fig. 1c).

In this paper, we investigate these new patterns by considering a one-dimensional system. In Section 2 we review the phase-field model and present the two-dimensional numerical simulations which give rise to concentric rings. A one-dimensional investigation is presented in Section 3. Three types of solutions are identified including uniformly translating fronts, Zener-like solutions, and oscillatory solutions. In Section 4, analytical approximate expressions are derived for the uniformly translating solutions, and for their range of existence. The oscillatory solutions are studied in Section 5. The oscillating wave-front is found to propagate into a new intermediate phase, its velocity and wavelength satisfying a marginal stability principle [16,17]. Concluding remarks are made in Section 6.

## 2. The phase-field model

### 2.1. The model

The phase-field model has become one of the standard models to describe pattern formation during diffusion limited growth [18,19]. It is based on a phenomenological description of the phase boundaries as a diffuse interface by means of a continuous order-parameter field. The order-parameter has two locally stable fixed points, identified as the thermodynamical phases (liquid and solid). Its dynamics is derived from a Landau free-energy by a variational principle. The dynamics of the order parameter is coupled to that of a diffusion field (e.g., temperature or concentration). The coupling between the two fields is on two levels. On the one hand, the diffusion field determines locally the relative stability of the two phases. On the other hand, variations in the order parameter act as a source for the diffusion field (latent heat generation in the thermal model, or absorption due to a miscibility gap in the chemical model).

The model considered here describes solidification of a pure substance from its undercooled melt. The order-parameter, $\phi$, is defined such that $\phi = 0$ in a homogeneous liquid, and $\phi = 1$ in a homogeneous solid. The conjugate temperature field, $T$, is represented by the dimensionless field, $u = c_p(T - T_M)/L$, where $T_M$ is the phase coexistence equilibrium temperature, $c_p$ is the specific heat, and $L$ is the latent heat per unit volume. The thermal properties of the substance are assumed to be equal in both phases (symmetric model). The dynamical evolution of the system is given by [20]

$$\frac{\xi^2}{\gamma}\frac{\Delta F(u)}{V(u)}\frac{\partial\phi}{\partial t} = \xi^2\nabla^2\phi + \phi(1-\phi)\left(\phi - \frac{1}{2} - \xi\frac{\Delta F(u)}{\sqrt{2}\gamma}\right), \tag{1}$$

and

$$\frac{\partial u}{\partial t} = D\nabla^2 u + \frac{\partial\phi}{\partial t}. \tag{2}$$

The parameters are related to the material properties as follows: $\xi$ is the thickness of the interfacial layer at phases coexistence, $\gamma$ is the (isotropic) surface-energy (in two dimensions it is a line-energy), and $D$ is the heat diffusion constant. The function $\Delta F(u)$ denotes the thermodynamical free-energy difference between liquid and solid at temperature $u$, and the function $V(u)$ denotes the kinetic response function. That is, the velocity at which a flat interface would propagate under controlled isothermal conditions. Boundary and initial conditions complete the model. Growth in an open geometry, for example, is realized by taking $\phi(\infty) = 0$ and $u(\infty) = \Delta < 0$ as boundary conditions. The initial conditions consist of a solid nucleus in an undercooled environment.

In the sharp boundary limit where the interfacial thickness, $\xi$, is much shorter than the characteristic diffusion length, $\ell = D/\hat{v}$ ($\hat{v}$ is a characteristic velocity of the phase boundary), Eqs. (1) and (2) reduce to the free boundary model [21,22]. It is defined by the linear diffusion equation,

$$\frac{\partial u}{\partial t} = D\nabla^2 u, \tag{3}$$

and supplemented by boundary conditions on the moving interface. Namely, heat conservation

$$D\,[\nabla u]\cdot\hat{n} = -v_n, \tag{4}$$

where the square brackets denote discontinuity across the interface, and $v_n$ is the normal velocity of the in-

terface. The generalized kinetic Gibbs-Thompson relation is

$$\Delta F(u_i) = -\frac{\Delta F(u_i)}{V(u_i)} v_n - \gamma\kappa, \tag{5}$$

where $u_i$ is the temperature at the interface, and $\kappa$ is the local curvature. Eq. (5) reduces to its standard form in the linear approximation, $V(u) = u/\beta$ and $\Delta F(u) = (L^2/c_p T_M)\, u$.

For large scale numerical simulations, it proved advantageous to choose a specific form of the model originally proposed by Kobayashi [11],

$$\epsilon^2 \frac{\partial \phi}{\partial t} = \epsilon^2 \nabla^2 \phi + \phi(1-\phi)\left(\phi - \tfrac{1}{2} - \epsilon \tanh \lambda u\right), \tag{6}$$

and

$$\frac{\partial u}{\partial t} = \nabla^2 u + \frac{\partial \phi}{\partial t}. \tag{7}$$

In these dimensionless equations, length is measured in units of $D/\hat{v}$, and time is measured in units of $D/\hat{v}^2$. The parameter $\epsilon$ is the ratio of the interfacial thickness, $\xi$, and the characteristic diffusion length $D/\hat{v}$.

### 2.2. *Numerical simulations for large undercooling*

In Ref. [15] we presented a numerical investigation of the late-stage growth of phase-field simulations in a two-dimensional open geometry. The main result was the identification of different "growth elements": dendrites, parity-broken dendrites, tip-splitting fingers and compact growth. Each growth element is characteristic to a distinct region of the parameters space.

In this study, we concentrate on the limit of very large undercooling, for which superheated solid is generated. Growth of superheated solid into undercooled melt is in general unstable. This instability leads to the spontaneous emergence of liquid domains behind the propagating front. For the parameters used in Ref. [15] the resulting pattern was that of liquid droplets (Fig. 1a). For a larger value of interfacial diffusivity, $\epsilon$, the liquid domains organize instead in a new structure consisting of a periodic array of concentric rings. Such typical rings structure is shown in Fig. 1b. Two fronts are identified: first, the solid front which propagates into the liquid, and behind, the wave-front of the rings structure. Both fronts advance at constant speeds, the solid–liquid front being the fastest. This pattern is observed for a limited range of undercooling. Above a critical undercooling the rings disappear, the propagating phase being instead an homogeneous superheated solid. Below a lower critical undercooling the solid front destabilizes, giving rise to radial tip-splitting growth (Fig. 1c).

The circular symmetry of the rings structure suggests its investigation by means of a purely one-dimensional analysis. The following sections are devoted to such an investigation. The quantitative agreement between the two-dimensional simulations and the one-dimensional analysis is presented in the discussion section.

## 3. Numerical results for a one-dimensional system

In this section we present numerical solutions of the phase-field equations for a one-dimensional system. In order to investigate the time-dependent behavior, and find the dynamically selected solutions, Eqs. (6) and (7) were integrated numerically using the Crank-Nicholson scheme. We start with melt ($\phi = 0$) undercooled at temperature $u = -\Delta$, except for a solid nucleus ($\phi = 1$) at zero temperature located at the origin. The system boundaries are taken to be reflecting. In practice, the particular choice of boundary conditions does not affect the growth as long as the diffusion layer is sufficiently far from the boundaries.

We performed time-dependent simulations for various values of $\Delta$ and $\epsilon$. Three regimes of late-stage growth are identified, corresponding to three regions on the $\epsilon$–$\Delta$ plane (Fig. 2):

(i) Uniformly translating fronts, where the two phases are connected by a sharp domain wall of width of order $\epsilon$. Such solutions are obtained for all values of undercooling greater than a critical value $\Delta_c \leq 1$. For values of undercooling less than one, the growing phase is a superheated solid at temperature $u = 1 - \Delta > 0$. For small values of $\epsilon$, $\Delta_c$ tends to unit undercooling as expected for the sharp boundary limit.

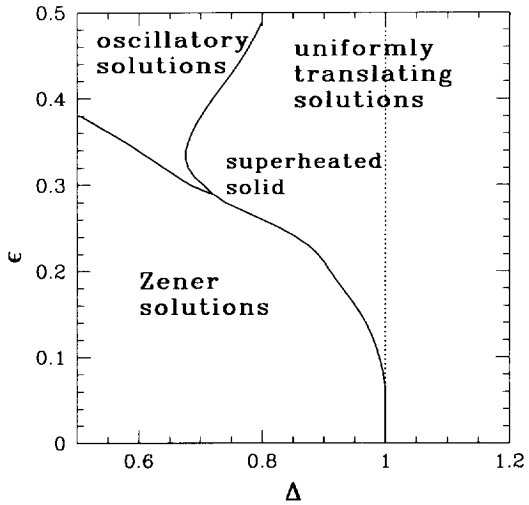


Fig. 2. Schematic map of the different late-stage growth regimes on the $\epsilon$–$\Delta$ plane.

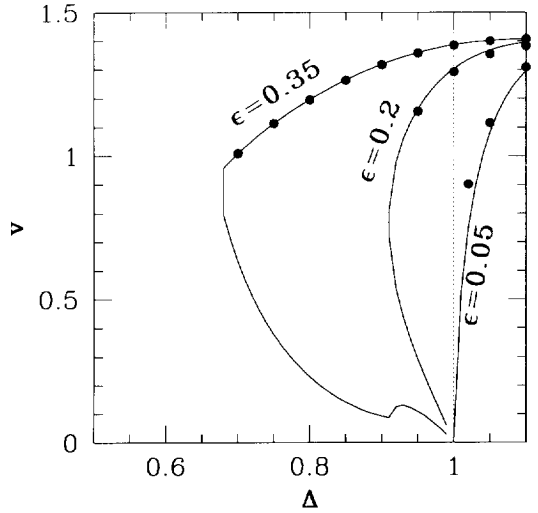


Fig. 3. Velocity of the uniformly translating fronts as function of undercooling for $\lambda = 10$ and for three different values of $\epsilon$. The solid lines are calculated using the shooting procedure. The dots are calculated from the time-dependent simulations.

For uniformly translating solutions, it is possible to solve directly the stationary equations in the moving frame. Eqs. (6) and (7) reduce then to

$$\epsilon^2\phi'' + \epsilon^2 v\phi' + f(\phi, u) = 0, \tag{8}$$

and

$$u'' + v(u' - \phi') = 0, \tag{9}$$

where $f(\phi, u) = \phi(1 - \phi)(\phi - 1/2 - \epsilon \tanh \lambda u)$. The boundary conditions are $\phi(-\infty) = 1$, $\phi(\infty) = 0$ and $u(\infty) = -\Delta$. The velocity of propagation, $v$, is determined by this non-linear eigenvalue problem. Integrating Eq. (9) once, we get

$$u' + v(u - \phi + \Delta) = 0, \tag{10}$$

where the constant of integration, $\Delta$, has been determined by the boundary conditions. It is useful to transform Eqs. (8) and (10) to a set of three first order equations, the third variable being $z = d\phi/dx$. The velocity, then, can be calculated numerically using a standard shooting method by requiring the existence of an integration path connecting the "solid" fixed point, $(\phi = 1, u = 1 - \Delta, z = 0)$, to the "liquid" fixed point, $(\phi = 0, u = -\Delta, z = 0)$. This velocity is presented in Fig. 3 as function of undercooling for different values of $\epsilon$. For $\Delta_c < \Delta < 1$, the velocity is multivalued, but only the upper branch for which $v$ is an increasing function of $\Delta$ is linearly stable.

(ii) Slowing down Zener-like solutions. In this regime the front slows down as $1/\sqrt{t}$, while the length of the thermal diffusion layer increases as $\sqrt{t}$. These solutions can be calculated analytically in the sharp boundary limit by means of a similarity transformation [23].

(iii) Oscillatory solutions. In this regime, the front advances at constant velocity although the level of undercooling is not sufficiently high to sustain uniform translation. The superheated solid left behind the front is unstable, and decomposes into a periodic structure of alternating regions of solid and liquid. These solutions are observed above a critical value of $\epsilon$, and for a range of undercooling which is bounded above by the regime of uniformly translating fronts, and bounded below by the regime of Zener solutions.

In Figs. 4a and 4b we show the fields profiles above (4a) and below (4b) a transition from uniformly translating fronts to Zener solutions. In both regimes

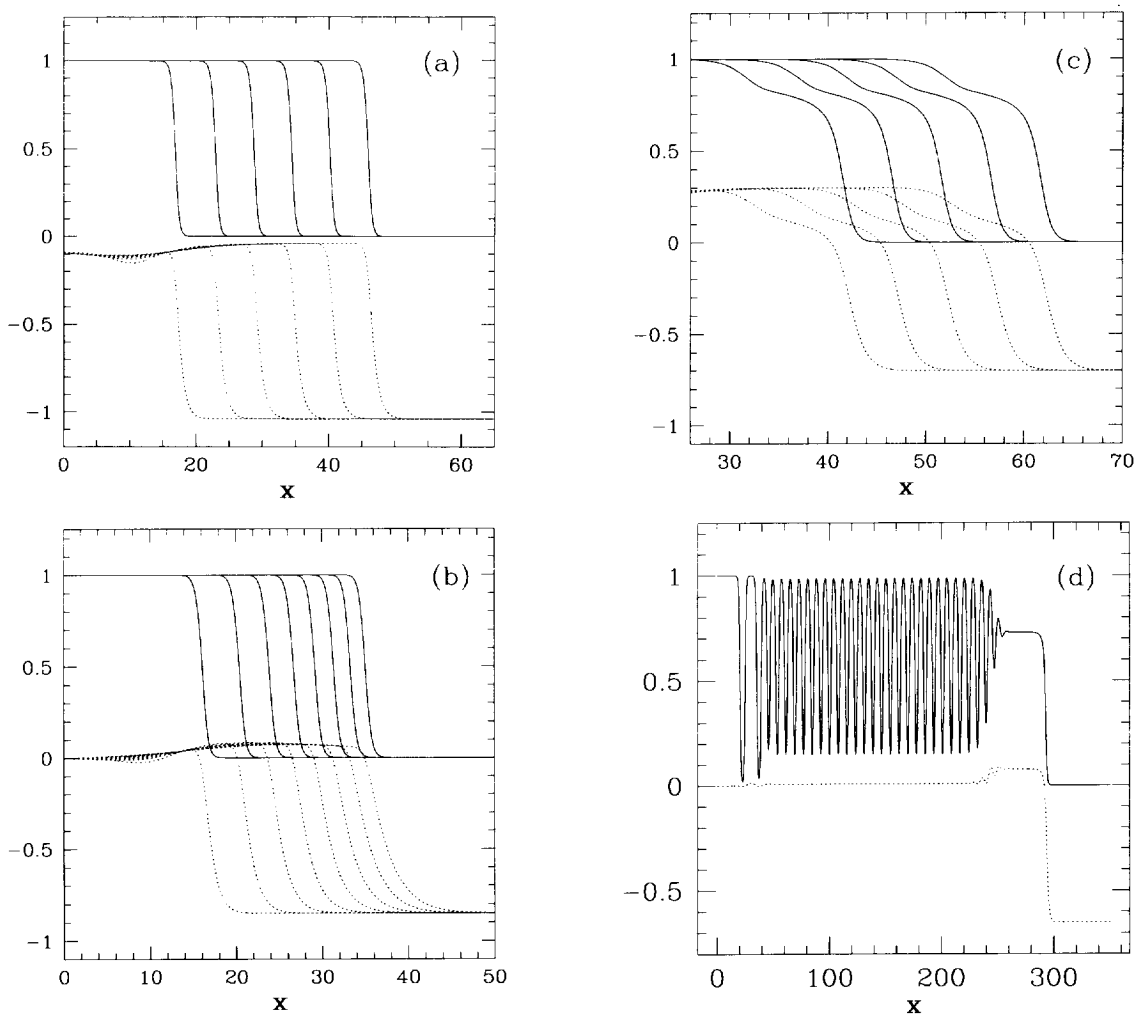


Fig. 4. Snapshots of the profiles of $\phi(x)$ (solid lines) and $u(x)$ (dotted lines). (a) and (b) are for $\lambda = 10$ and $\epsilon = 0.2$, and show a transition from a uniformly translating front (a) to the Zener regime (b). (c) and (d) are for $\lambda = 10$ and $\epsilon = 0.35$, and show a transition from a uniformly translating front (c) to the oscillatory regime (d).

the front is sharp, its width being of order $\epsilon$. This is not the case in the vicinity of a transition from a uniformly translating front to an oscillatory solution (Figs. 4c and 4d). For $\Delta \gtrsim \Delta_c$ (Fig. 4c), the front is structured. Both $\phi(x)$ and $u(x)$ pass through a saddle point, so that the profile is effectively divided into two rapidly varying regions which are connected through a moderately varying region. As $\Delta$ approaches $\Delta_c$ from above, the region where the fields are nearly constant widens. For $\Delta < \Delta_c$ (Fig. 4d), the profile divides into two separated regions. A uniformly translating front connects the liquid to an "intermediate phase" (a meta-stable state for which $0 < \phi < 1$). Behind this front, the periodic pattern propagates into the intermediate phase. A secondary process of period doubling occurs far behind the wave-front, indicating that the wave-pattern is not a globally stable state.

The new solution of a front connecting the liquid phase to the intermediate phase bifurcates off the uniformly translating solutions of solid–liquid fronts. Fig. 5 shows that the $v(\Delta)$ curve of the former originates from the upper branch of the latter.

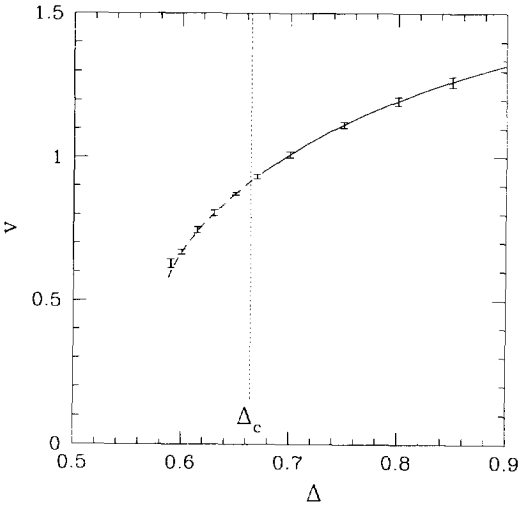


Fig. 5. Velocity versus undercooling for $\lambda = 10$, and $\epsilon = 0.35$. The critical undercooling is $\Delta_c \simeq 0.686$. The solid line represents the velocity of the uniformly translating solid–liquid fronts, whereas the dashed line gives the velocity of the front connecting the liquid phase to the intermediate phase. Both are calculated using the shooting procedure as explained in Section 4. The bars represent the data extracted from the time-dependent simulations.

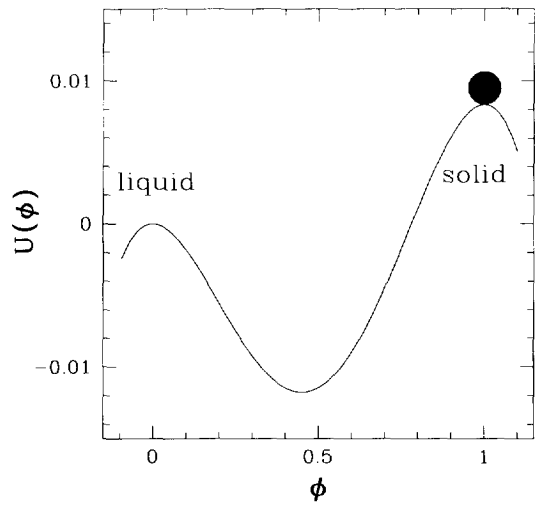


Fig. 6. The mechanical analog: the particle trajectory connects the unstable equilibrium points, $\phi = 1$ and $\phi = 0$.

## 4. Phase-space representation

### 4.1. Mechanical analog of the phase-field equations

A standard procedure in the analysis of front propagation is to refer to an analogous mechanical system. Here we present a generalization of the standard analogy in order to gain additional insight about the new phenomena described above. First, we consider Eqs. (8) assuming $u$ being constant. It can be viewed as describing the motion of a particle of mass $\epsilon^2$, $\phi$ being its displacement, $x$ being time and $\epsilon^2 v$ being the dissipation constant. The particle is driven by a force, $f(\phi, u)$, derived from the potential

$$U(\phi, u) = -\tfrac{1}{4}\phi^2(1-\phi)^2 - \left(\tfrac{1}{2}\phi^2 - \tfrac{1}{3}\phi^3\right)\epsilon \tanh(\lambda u), \qquad (11)$$

which equals to minus the potential part of the free-energy. Hence, it has two maxima, at $\phi = 0$ and at $\phi = 1$, and a local minimum at $\phi = 0.5 + \epsilon \tanh(\lambda u)$ (Fig. 6). The fictitious particle moves along the homoclinic trajectory connecting the "solid" unstable equilibrium point, $\phi = 1$, to the "liquid" unstable equilibrium point, $\phi = 0$. This analogy can be employed to calculate the velocity of propagation, $v$, using energy conservation. Under the assumption of constant temperature, there exists a unique trajectory, and hence only one possible velocity.

Next, we combine the above picture with the simultaneous evolution of $u(x)$. The integration of Eq. (10) gives

$$u(x) = \phi(x) - \Delta - e^{-vx}\int_{-\infty}^{x} ds\, e^{vs}\frac{\partial \phi}{\partial x}(s). \qquad (12)$$

The particle's trajectory can be described now in the following manner. While the particle moves towards $\phi = 0$, $u$ evolves according to Eq. (12). The potential, $U(\phi, u)$, varies consequently, with the maximum at $\phi = 1$ shifting upwards while the minimum at $\phi = \frac{1}{2} + \epsilon \tanh \lambda u$ moves towards the left. The energy conservation relation has also to account now for the energy gained by the potential shift along the trajectory. It is the possibility of such energy gain to compensate the negative potential difference between the initial and the final states which allows the formation of superheated solid.

The energy conservation law is

$$\epsilon^2 v \int_{-\infty}^{\infty} dx \left(\frac{\partial \phi}{\partial x}\right)^2 = \epsilon \int_{-\infty}^{\infty} dx \tanh(\lambda u)\phi(1-\phi)\frac{\partial \phi}{\partial x}. \quad (13)$$

The function $v(\Delta)$ can be estimated by performing the following approximation. As $\phi$ decays from 1 to 0 over a distance of order $\epsilon$, it is a reasonable approximation to replace it by a model function,

$$\phi_M(x) = \begin{cases} 1 - \frac{1}{2}\exp\left(\frac{x}{\alpha\epsilon}\right) & x < 0 \\ \frac{1}{2}\exp\left(-\frac{x}{\alpha\epsilon}\right) & x > 0 \end{cases}, \quad (14)$$

where $\alpha$ is a fitting parameter. From the integral expression for $u$, Eq. (12), it follows that the temperature also varies mainly in the region $x \sim O(\epsilon)$ where $\partial\phi/\partial x$ is large. Hence, we replace $\tanh(\lambda u)$ by a power series in $\epsilon$ about $x = 0$. Substituting this power series expansion together with the model function, $\phi_M(x)$, into Eq. (13), we obtain

$$v = -\frac{2\alpha}{3}\tanh[\lambda u(0)] + O(\epsilon^2). \quad (15)$$

The front velocity is determined within this approximation by the temperature at the interface. To set the fitting parameter, $\alpha$, we compare this result with the sharp boundary limit, $v = -\sqrt{2}\tanh[\lambda u(0)]$. Hence, $\alpha = 3/\sqrt{2}$. Finally, $u(0)$ is evaluated by substituting the model function also into Eq. (12). This procedure gives an implicit equation for the front velocity,

$$v = \sqrt{2}\tanh\left\{\lambda\left[\Delta - \frac{1}{2} - \frac{1}{2(3\epsilon v/\sqrt{2}+1)}\right]\right\}. \quad (16)$$

The qualitative similarity between the evaluated velocity and the exact solution is shown in Fig. 7. Eq. (16) has multivalued solutions only if $\epsilon\lambda > 2/3$, which provides an estimate for the existence range of uniformly translating fronts which generate superheated solid.

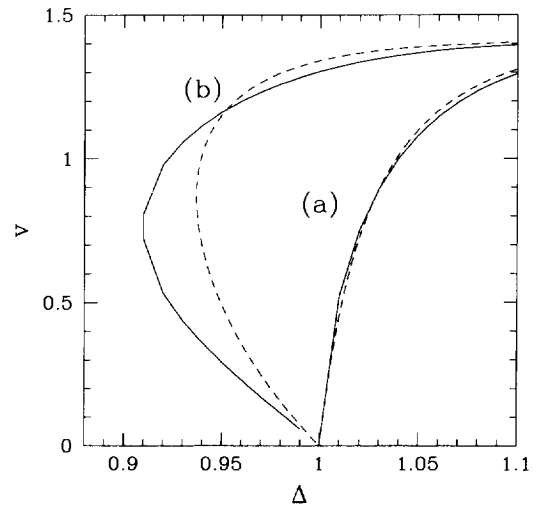


Fig. 7. Comparison between the exact velocity curves obtained using the shooting procedure (solid lines), and the approximated solution (dashed lines). For $\epsilon = 0.05$ (a) the agreement is excellent, but remains essentially qualitative for $\epsilon = 0.2$ (b).

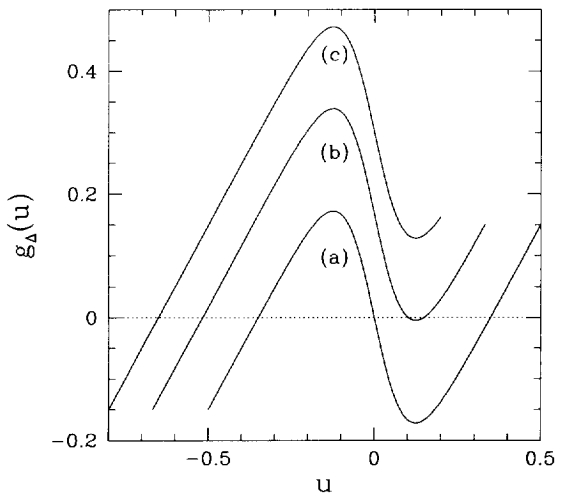


Fig. 8. The function $g_\Delta(u)$ for (a) $\Delta = 0.5$; (b) $\Delta = 0.667$ and (c) $\Delta = 0.8$.

### 4.2. The intermediate phase

Next, we turn to explain the formation of the new intermediate phase by considering the dynamical system which generates the profiles of the uniformly translating fronts,

$$\begin{cases} \dot{\phi} = z \\ \dot{z} = -vz - \frac{1}{\epsilon^2} f(\phi, u) \\ \dot{u} = v(\phi - u - \Delta) \end{cases}. \quad (17)$$

The relevant trajectories are those connecting the fixed point $(1, 0, 1-\Delta)$ to the fixed point $(0, 0, -\Delta)$. Local

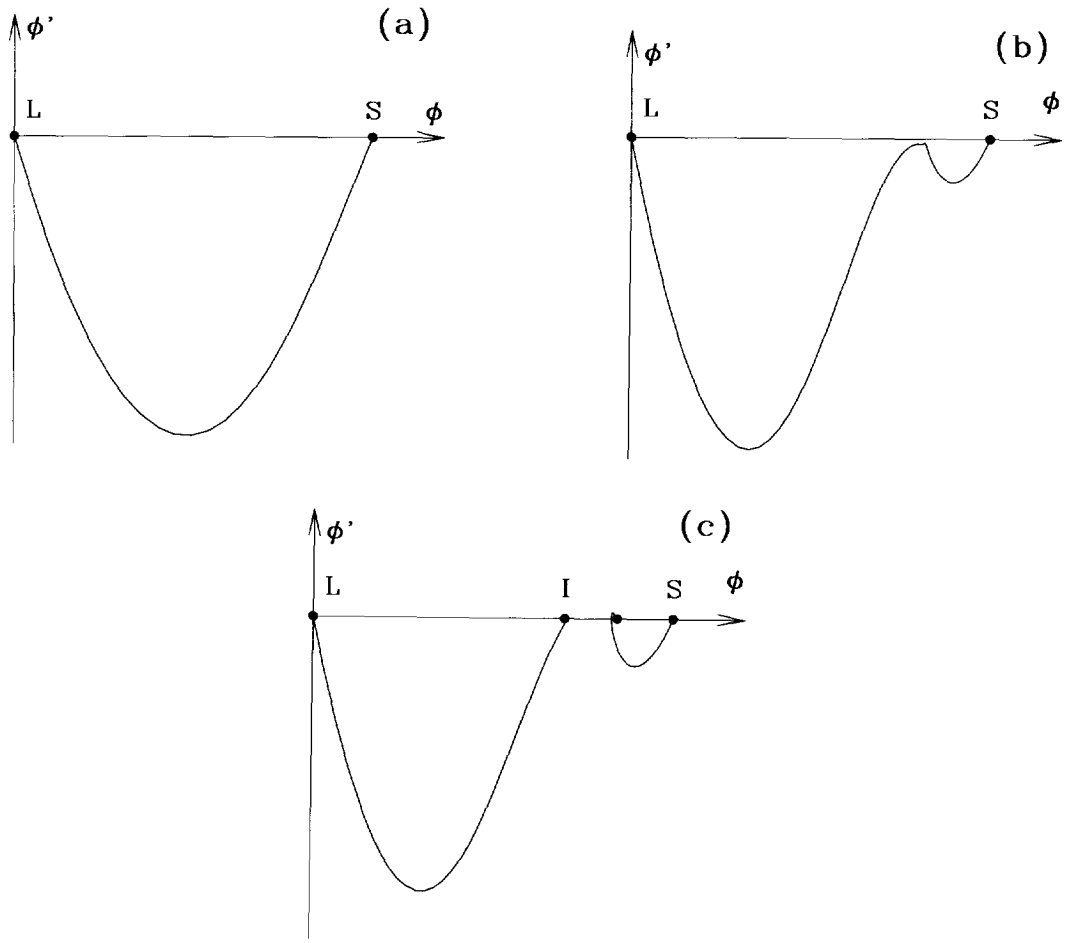


Fig. 9. Trajectories of the dynamical system (19) projected on the $\phi$–$z$ plane ($z = \phi'$). The parameters are $\epsilon = 0.35$, $\lambda = 10.0$ and (a) $\Delta = 1.0$; (b) $\Delta = 0.68$; (c) $\Delta = 0.64$.

analysis shows that both fixed points have two negative and one positive eigenvalues. A simple "counting argument" indicates that such trajectories will exist only for selected values of $v$, as the one trajectory leaving the point $(1, 0, 1 - \Delta)$ will in general (i.e., for arbitrary $v$) be on the one-dimensional unstable manifold of trajectories passing through the point $(0, 0, -\Delta)$.

The intermediate phase corresponds to an additional fixed points of Eq. (17), which is the root of

$$g_\Delta(u) \equiv u + \Delta - \tfrac{1}{2} - \epsilon \tanh(\lambda u) = 0. \qquad (18)$$

In Fig. 8 we plot $g_\Delta(u)$ for three values of $\Delta$. For $\Delta > \Delta_c$, Eq. (18) has only one root corresponding to the unstable fixed point (the stability is defined with respect to the rest frame for time dependent perturbations). For $\Delta = \Delta_c$, a saddle-node bifurcation gives rise to two additional roots. The stability of these new fixed points is determined by the sign of $g'_\Delta(u)$, hence, it is the middle one which corresponds to the intermediate phase.

Fig. 9 shows different trajectories of the dynamical system, (17) (the trajectories are projected on the $\phi$-$z$ plane). For $\Delta$ slightly larger than $\Delta_c$ (Fig. 9b), $z = \partial\phi/\partial x$ becomes very small in the vicinity of $\phi = 0.8$, reflected as a slowly varying region in terms of $\phi(x)$ (Fig. 4c). The $\Delta = \Delta_c$ trajectory is the first which

passes through the new fixed point, while there are no trajectories connecting the solid phase ($S$) to the liquid phase ($L$) for $\Delta$ below $\Delta_c$.

For $\Delta = \Delta_c$ the trajectory passes through a fixed point, and it corresponds to two independent fronts: one connecting $S$ to the intermediate state ($I$), and a second connecting the latter to $L$. The stability properties of $I$ being identical to those of $S$, we can find uniformly translating $I$–$L$ fronts using the same shooting procedure as for the $S$–$L$ fronts (Fig. 9c). The velocity curve of these fronts was shown in Fig. 5 to bifurcate off the $S$–$L$ fronts velocity curve. A similar attempt to find $S$-$I$ fronts failed as all the trajectories leaving $S$ flow into the *unstable* intermediate fixed point. Thus, uniformly translating $S$-$I$ fronts don't exist, in agreement with the numerical simulations.

## 5. Velocity and wavelength selection in the oscillatory regime

Having treated separately the $I$–$L$ front propagation, we analyze in this section the formation and the propagation of the periodic state into the $I$-state. Behind the oscillations wave-front, the periodic pattern is stationary. So far, the only stationary states which were considered were homogeneous ones, however the phase-field equations assume also periodic solutions. The stationary equations are

$$u = u_0 = \text{Const.}, \tag{19}$$

and

$$\epsilon^2\phi'' + f(\phi, u) = 0, \tag{20}$$

so that Eq. (20) can be identified as describing the frictionless motion of a particle of mass $\epsilon^2$ in the potential field, $U(\phi, u_0)$, $\phi$ being again the analog of displacement. The corresponding energy conservation law is

$$\tfrac{1}{2}\epsilon^2(\phi')^2 + U(\phi, u_0) = E. \tag{21}$$

Provided that the total energy, $E$, is less than the energy of the potential barriers, (i.e., $E < U(0, u_0), U(1, u_0)$), the solution will be that of periodic oscillations about the minimum of $U(\phi, u_0)$. The apparent two-parameters ($u_0$ and $E$) family of periodic solutions is reduced to a one-parameter family under the constraint of global heat conservation. Comparing the periodic solution with the homogeneous intermediate state, $(\phi^*, u^*)$, the difference in $\phi(x)$ must on the average be equal to the difference in $u(x)$. That is,

$$\frac{1}{\lambda^*}\int_x^{x+\lambda^*} dx' \left[\phi(x') - \phi^*\right] = u_0 - u^*, \tag{22}$$

where $\lambda^*$ is the wavelength of the periodic pattern.

The existence of a continuous family of periodic solutions poses a selection problem, both for the wavelength and for the velocity at which the oscillatory pattern advances into the intermediate state. It will be shown that the selection mechanism satisfies a marginal stability principle which is characteristic to cases where a stable phase propagates into an unstable one. Such problems were extensively studied by Ben-Jacob et al. [16] and by Van Saarloos [17].

Consider a general disturbance propagating into the intermediate state. The assumption is that the selection is completely determined at the leading edge of this disturbance. There, we can take a perturbation of the form,

$$\begin{aligned} \phi(x,t) &= \phi^* + \delta\phi\, \exp(\omega t - kx) \\ u(x,t) &= u^* + \delta u\, \exp(\omega t - kx) \end{aligned}, \tag{23}$$

and linearize the equations about the intermediate state. The following dispersion relation is obtained

$$\omega(k) = k^2 + \frac{1}{2\epsilon^2}(f_\phi + f_u) \pm \frac{1}{2\epsilon^2}\sqrt{(f_\phi + f_u)^2 + 4\epsilon^2 k^2 f_u} \tag{24}$$

(the solution is dominated by the positive root), where

$$f_\phi = \left.\frac{\partial f}{\partial \phi}\right|_{\phi^*, u^*} = \phi^*(1 - \phi^*), \tag{25}$$

and

$$f_u = \left.\frac{\partial f}{\partial u}\right|_{\phi^*, u^*} = -\epsilon\lambda\frac{\phi^*(1-\phi^*)}{\cosh^2(\lambda u^*)}. \tag{26}$$

In general, both $k$ and $\omega$ are complex. The enve-

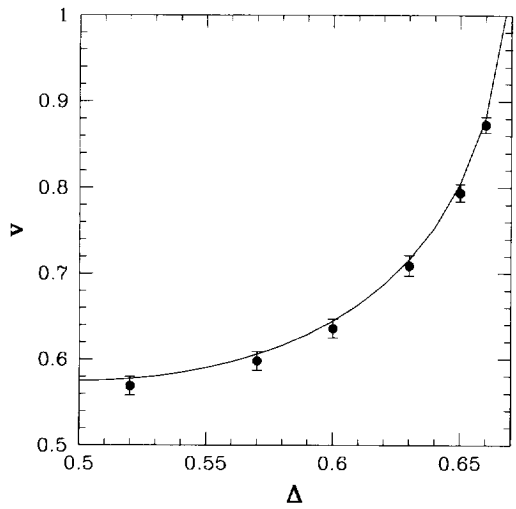


Fig. 10. The velocity at which the oscillations wave-front propagates into the intermediate phase for $\epsilon = 0.35$ and $\lambda = 10$. The solid curve is calculated using the marginal stability hypothesis. The dots are results of numerical simulations.

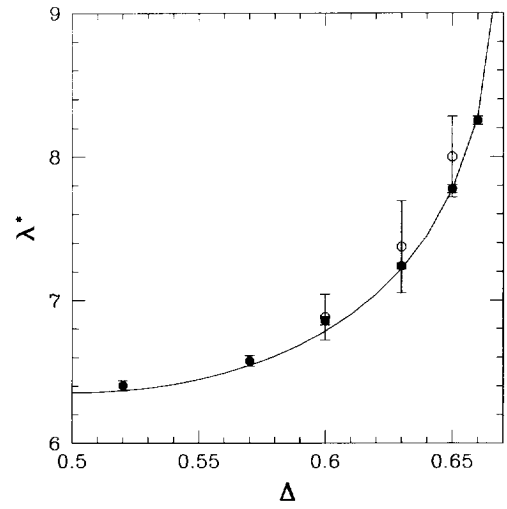


Fig. 11. Wavelength of the periodic pattern as function of undercooling for $\epsilon = 0.35$ and $\lambda = 10$. The solid curve is calculated using the marginal stability hypothesis. The solid dots are the results of the one-dimensional numerical simulations, whereas the open dots are the wavelength of the concentric pattern in the two-dimensional simulations.

lope of the disturbance is determined by Re $k$ and its velocity is given by

$$c(k) = \frac{\mathrm{Re}\ \omega(k)}{\mathrm{Re}\ k}. \tag{27}$$

Imagine now a superposition of such Fourier components, all having the same value of Re $k$ (i.e., spatial decay), but different values of Im $k$. Clearly, the solution will be dominated after long time by the mode which maximizes the velocity of the envelope. Therefore, rather than being viewed as an independent degree of freedom, Im $k$ can be considered to be a function of Re $k$ through the condition that

$$\left.\frac{\partial c(k)}{\partial\,\mathrm{Im}\ k}\right|_{\mathrm{Re}\ k} = 0, \quad \text{hence} \quad \left.\frac{\partial\,\mathrm{Re}\ \omega(k)}{\partial\,\mathrm{Im}\ k}\right|_{\mathrm{Re}\ k} = 0. \tag{28}$$

An additional condition has to determine the selected decay rate of the envelope. It can be derived in various alternative manners. Perhaps the most intuitive approach is the one adopted by Van Saarloos [17]. Provided that the initial perturbation is sufficiently localized, the construction of the envelope can be thought of as consisting of a continuous process in which the front is being "invaded" from behind by modes of longer spatial decay. This process continues as long as the long spatial decay modes are slower. Once the velocity has reached a minimum, the front remains stable with respect to such "invasions". Hence, the condition for the selected spatial decay rate is

$$\frac{dc}{d\,\mathrm{Re}\ k} = \frac{1}{\mathrm{Re}\ k}\frac{d\,\mathrm{Re}\ \omega}{d\,\mathrm{Re}\ k} - \frac{\mathrm{Re}\ \omega}{(\mathrm{Re}\ k)^2} = 0, \tag{29}$$

and since

$$\frac{d\,\mathrm{Re}\ \omega}{d\,\mathrm{Re}\ k} = \frac{\partial\,\mathrm{Re}\ \omega}{\partial\,\mathrm{Re}\ k} + \frac{\partial\,\mathrm{Re}\ \omega}{\partial\,\mathrm{Im}\ k}\frac{d\,\mathrm{Im}\ k}{d\,\mathrm{Re}\ k} = \frac{\partial\,\mathrm{Re}\ \omega}{\partial\,\mathrm{Re}\ k},$$

we obtain the second condition that

$$\frac{\partial\,\mathrm{Re}\ \omega}{\partial\,\mathrm{Re}\ k} = \frac{\mathrm{Re}\ \omega}{\mathrm{Re}\ k}. \tag{30}$$

Eqs. (24), (28) and (30) determine the marginally stable mode, $k = k_{\mathrm{MS}}$, together with the velocity of propagation, $c_{\mathrm{MS}}$. In order to calculate the wavelength of the oscillations, $\lambda^*$, we use the standard node-counting argument [16]. In a frame of reference moving with the envelope at speed $c_{\mathrm{MS}}$, the rate at which nodes are created at the leading edge is given by $\frac{1}{\pi}\,\mathrm{Im}\,(\omega_{\mathrm{MS}} - c_{\mathrm{MS}}k_{\mathrm{MS}})$. Assuming that nodes are neither created nor annihilated elsewhere than at the leading edge, this rate is equal to $2c_{\mathrm{MS}}/\lambda^*$, which is the rate at which nodes are passing through a second comoving observation point which is located in the de-

veloped waveform. This determines the wavelength to be,

$$\lambda^* = 2\pi \left[ \mathrm{Im} \left( \frac{\omega_{\mathrm{MS}}}{c_{\mathrm{MS}}} - k_{\mathrm{MS}} \right) \right]^{-1}. \quad (31)$$

The calculated values of $c_{\mathrm{MS}}$ and $\lambda^*$ are compared with the simulations data in Figs. 10 and 11. The agreement is very good, showing conclusively that marginal stability governs the selection of the periodic solutions.

## 6. Conclusions

We studied the propagation of superheated solid into undercooled melt at large undercooling in the framework of the phase-field model. Such propagation leads to a decomposition of the superheated solid into alternating liquid and solid domains, constrained by the equality of the average solid fraction and the dimensionless undercooling. In the regime where the growth in two-dimensional gives rise to concentric rings, a one-dimensional investigation provides a good estimate for the wave-length of the periodic structure (Fig. 11), and for its velocity of propagation (Fig. 10). The periodic solution breaks down in both one-dimensional and two-dimensional case for the same critical value of undercooling. While in 1D, this transition yields a solution in which the front slows down, in 2D, the solidification front has the possibility to keep growing at constant rate by selecting a new growth pattern. As a result, the growth morphology undergoes a transition to tip-splitting growth, that is, the character of the structure changes from concentric to radial.

While this analysis is interesting mathematically, its physical significance is not clear. As a model of solidification, the layer of the phase must be thin, and cannot admit internal structures. Different is the application of a phase-field model to superconducting-to-normal transitions (there, the two fields vary over comparable scales). It remains to find whether our results have physical relevance to the formation of liquid domains behind a solidification front. The major difficulty lays in the fact that levels of undercooling (or alternatively, levels of supersaturation) as large as $\Delta = 0.7$–$0.9$ are hard to attain. Relatively large undercooling has been realized in liquid crystals and in white phosphorus [24] due to their small latent heat, hence they seem to be the most promising systems for the performance of large undercooling experiments.

## Acknowledgements

We are grateful to D. Kessler, Z. Schuss and R. Mints for useful discussions. This study was supported in part by a grant from the G.I.F., the German-Israeli Foundation for Scientific Research and Development, and by grant No. 9200051 from the United States-Israel Binational Science Foundation (BSF).

## References

[1] D.A. Kessler, J. Koplik and H. Levine, Adv. Phys. 37 (1988) 255.
[2] J.S. Langer, Science 243 (1989) 1150.
[3] E. Ben-Jacob and P. Garik, Nature 343 (1990) 523.
[4] E.A. Brener and V.I. Mel'nikov, Adv. Phys. 40 (1991) 53.
[5] M.E. Glicksman, R.J. Schaefer and J.D. Ayers, Metall. Trans. A 7 (1976) 1747.
[6] O. Shochet, K. Kassner, E. Ben-Jacob, S.G. Lipson and H. Müller-Krumbhaar, Physica A 181 (1992) 136; A 197 (1992) 87.
[7] E.A. Brener, H. Müller-Krumbhaar and D.E. Temkin, Europhys. Lett. 17 (1992) 535.
[8] M. Ben-Amar and Y. Pomeau, Europhys. Lett. 2 (1986) 307.
[9] D.A. Kessler, J. Koplik and H. Levine, Phys. Rev. A 33 (1986) 3352.
[10] D.A. Kessler and H. Levine, Phys. Rev. A 33 (1986) 2612, 2634.
[11] Ryo Kobayashi, Physica D 63 (1993) 410.
[12] A.A. Wheeler, B.T. Murray and R.J. Schaefer, Physica D 66 (1993) 243.
[13] T. Ihle and H. Müller-Krumbhaar, Phys. Rev. Lett. 70 (1993) 3083.
[14] T. Ihle and H. Müller-Krumbhaar, Phys. Rev. E 49 (1994) 2972.
[15] R. Kupferman, O. Shochet and E. Ben-Jacob, Phys. Rev. E 50 (1994) 1005.
[16] E. Ben-Jacob, H. Brand, G. Dee, L. Kramer and J.S. Langer, Physica D 14 (1985) 348.
[17] W. van Saarloos, Phys. Rev. A 37 (1988) 211; A 39 (1989) 6367.
[18] J.B. Collins and H. Levine, Phys. Rev. B 31 (1985) 6119.

[19] J.S. Langer, in: Directions in Condensed Matter Physics, G. Grinstein and G. Mazenko, eds. (World Scientific, 1986).
[20] Raz Kupferman, unpublished.
[21] G. Caginalp and P.C. Fife, Phys. Rev. B 33 (1986) 7792; SIAM J. Appl. Math. 48 (1986) 506.
[22] Raz Kupferman, O. Shochet, E. Ben-Jacob and Zeev Schuss, Phys. Rev. B 49 (1992) 16045.
[23] V.K. Pinus and P.L. Taylor, Phys. Rev. B 32 (1985) 5362.
[24] M.E. Glicksman and R.J. Schaefer, J. Cryst. Growth 1 (1967) 297.